Spherical Fourier Cell and Application for Optical True Time Delay

David J. Rabb, Betty Lise Anderson, *Senior Member, IEEE, Member, OSA*, William D. Cowan, *Senior Member, IEEE*, and Olga Blum Spahn, *Member, IEEE*

***Abstract*—A new optical configuration for switching light beams called a spherical Fourier cell is explained. Its use for optical true time delay is outlined. An experimental apparatus was constructed for a 6–bit delay system, with 2 bits demonstrated. Delays of 0, 2.1, 4.1, and 6.2 ns were measured. Loss and crosstalk measurements are also given.**

***Index Terms*—Beam forming, Fourier optics, optical signal processing, optical time delay, phased array antenna.**

I. Introduction

A SPHERICAL Fourier Cell, introduced here, is an optical imaging system which can be used as a switching engine for parallel optical signal processing of an array of inputs. A central spherical lens is used by all beam paths within the switching engine. This allows for the system to be very compact as beams are free to overlap within and around the central "ball" lens. By imaging an array of inputs on to spatial light modulators beam paths can be controlled separately, enabling the switching engine to affect beams independently.

Time delay networks are of importance in the area of phased array radars. A single antenna element produces a very divergent signal; when an array of elements is used and signals are combined coherently the outgoing beam is much narrower, enabling more distant communication. To steer the beam the timing of the signal for various elements can be altered so that the direction of propagation is changed. For smaller bandwidth RF signals this can be accomplished through the use of phase shifting, but this only works for a single frequency while other frequencies experience beam squint and are sent at different angles. Using a true time delay approach, all frequencies receive the same delay and propagate in the same direction, thus allowing for much greater bandwidth. These time delays can be accomplished in the RF domain, for example RF MEMS [1] which use coplanar waveguides. For longer delays this approach becomes lossy ($\sim$10 dB/nsec), and for systems with large numbers of antenna elements ($\sim$1000) and a large number of delays required ($\sim$100), performing the delays in the RF domain can become quite bulky.

To reduce loss one could impose the RF signal onto an optical carrier and then perform delays in the optical domain. One such example would be a network of fibers of varying lengths with a series of optical switches [2], but again with fibers required for each element and each delay the system can become quite bulky. To reduce the number of elements chirped gratings can be used, but this requires the use of a tunable laser for each input as well as narrow bandwidth filters (possibly tunable) at the output. Instead of implementing delays in a guided media they could be done in free space, where one delay path can be used by a large number of optical carriers, all of which are separately controlled. One such approach is based on a White Cell [3], which was originally used for spectroscopy, but with addition of an optical MEMS and imaging arms of varying lengths can be used to implement independently controlled delays on an array of optical beams [4].

We propose here another free space approach, called the spherical Fourier cell. It is more compact than a White cell with similar delays because the central spherical lens is shared by all beam paths. The purpose of this system is to provide true time delays (TTDs) for an input array of light beams, and to independently control the amount of time delay each beam receives relative to a given minimum delay for the system. Unlike other systems using chirped fibers, delay is not wavelength dependent, so more simplified sources and detectors may be used.

First, in Section II the principal of operation will be discussed. A spherical lens (ball) will be introduced along with equations showing how to use it as the lens for a Fourier transform. Light beams will pass through this spherical lens multiple times in a specific pattern, imaging on one side of the system. We will also show how to set up mirrors around the sphere to get the desired bounce pattern. We will introduce a two-dimensional fiber array at the input along with microelectromechanical systems (MEMS) chips at subsequent image planes. At the Fourier transform planes we will separate mirrors into two sections, one a flat mirror and the other a delay device such as a glass block or lens train that has a delay associated with it. We will explain how the MEMS pixels control whether a beam is delayed or is sent to the null delay mirror. Various types of delay implementations are also discussed. Section III outlines the experimental apparatus used for the Fourier cell proof of concept, including the experimental results including delay, loss, and crosstalk measurements. Section IV is a summary of the results.

Manuscript received December 11, 2007; revised May 9, 2008. Current version published April 17, 2009.

D. J. Rabb is with the Air Force Research Laboratory, Wright Patterson AFB, OH 45433 USA (e-mail: david.rabb@wpafb.af.mil).

B. L. Anderson is with The Ohio State University, Columbus, OH 43210 USA (e-mail: anderson@ece.osu.edu).

W. D. Cowan and O. B. Spahn are with Sandia National Laboratories, Albuquerque, NM 87185 USA (e-mail: wdcowan@sandia.gov; oblum@sandia.gov).

Digital Object Identifier 10.1109/JLT.2008.927762

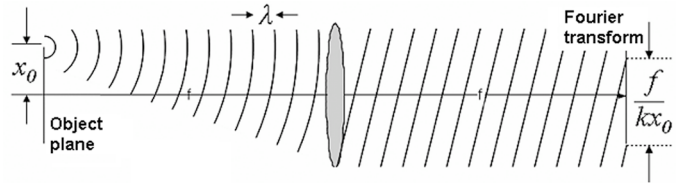

Fig. 1. Fourier transform; Phase fronts and spatial frequency.

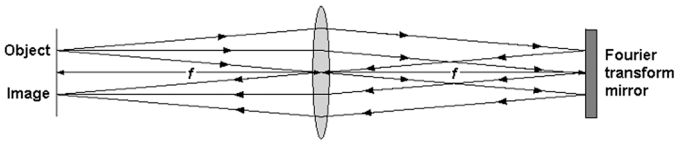

Fig. 2. Point source imaged at the object plane.

II. Principle of Operation

A. Switching Engine

We break up the explanation of the Fourier cell into two parts, first the switching engine that controls the paths of the beams, then the delay elements. The spherical Fourier cell is an imaging system that extensively uses the optical Fourier transform. A lens that has a focal length f, and is separated by a distance f along the lens optical axis from an object plane, will have an optical Fourier transform located a distance f along the optical axis on the opposite side of the lens. The result of this is that the position of the light in the input plane dictates the spatial frequency in the output plane, and conversely the spatial frequency at the input dictates position at the transform.

We can represent plane waves with rays normal to wave fronts. If a flat mirror is placed at the plane of the Fourier transform, the light is reflected back through the lens and the transform of the transform is located at the original object plane. This situation is depicted in Fig. 2. The result is the image of the object at the same plane as the object but on the opposite side of the optical axis of the mirror in the transform plane.

For our particular case we are going to be using beams coming out of single-mode fibers, which closely match Gaussian profiles. We therefore want to look at the Fourier transform, considering the input to be Gaussian. The Fourier transform of a Gaussian beam at its waist is another Gaussian beam at its new waist. If the radius of the input beam is w_1 and the radius of the beam at the output is w_2, the relationship between the input spot radius and the output spot radius can be found for a particular focal length f, and the wavelength of the light λ

$$w_2 = \frac{\lambda f}{\pi w_1}. \tag{2}$$

If a flat mirror is put at the transform plane the beam will come to a waist again at the object plane with the same radius as the input. Both rays and Gaussian beams are imaged back at the object plane with a magnification equal to -1 (the image is inverted). Since the system is symmetric about the lens, the same could be said if the beam originated at the transform side and there were a mirror at the object plane.

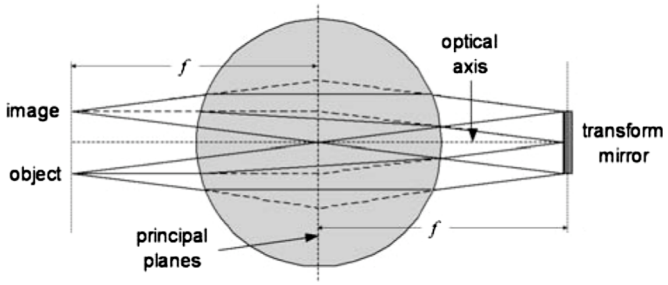

Fig. 3. Sphere with mirror at transform.

Although we have shown a thin lens in Figs. 1 and 2 in our application we will be using a spherical lens that will not be thin. In order to use the thin lens approximations we need to find the front and back principal planes of the sphere using ray matrices. The paraxial system matrix for the sphere consists of refraction at the surface on either side along with a translation between the surfaces, equal to the sphere's diameter, shown in (1). Here we are assuming free space around the sphere, a refractive index n inside the sphere, and that the sphere has a radius R

$$\begin{aligned}\begin{bmatrix} A & B \\ C & D \end{bmatrix} &= \begin{bmatrix} 1 & 0 \\ (1-n)/R & 1 \end{bmatrix} \begin{bmatrix} 1 & 2R/n \\ 0 & 1 \end{bmatrix} \begin{bmatrix} 1 & 0 \\ (1-n)/R & 1 \end{bmatrix} \\ &= \begin{bmatrix} (2-n)/n & 2R/n \\ 2(1-n)/nR & (2-n)/n \end{bmatrix}. \end{aligned} \tag{1}$$

Using this system matrix the principal planes can be found. The results indicate that both the front and back principal planes are a distance R inside the sphere, meaning they are both at the center. So if we have an input a distance f from the front principal plane, the Fourier transform can be found a distance f from the back principal plane, where f is the focal length of the sphere. The focal length of the sphere can be calculated using

$$f = -\frac{1}{C} = -\frac{nR}{2(1-n)} = \frac{nR}{2(n-1)} \tag{2}$$

where C is the (2,1) element of the paraxial ray matrix in (1). For our case, we want the focal planes to be outside of the sphere ($f > R$) and the focal length should not be negative. Assuming free space around the sphere, the refractive index n of the sphere can therefore be between 1 and 2.

It has been shown that a mirror at the Fourier transform normal to the optical axis results with an image on the opposite side of the optical axis from the object. In the case of a sphere, there are infinite possible optical axes normal to both surfaces of the sphere; the one about which the object is imaged is the one normal to the mirror at the transform plane (situation is depicted in Fig. 3). Along any of these axes the principal planes are in the center of the sphere with focal planes a distance f from the center on either side.

In Fig. 3, the solid lines indicate actual ray paths; dashed lines are ray paths for a thin lens at the principal planes, and the dotted

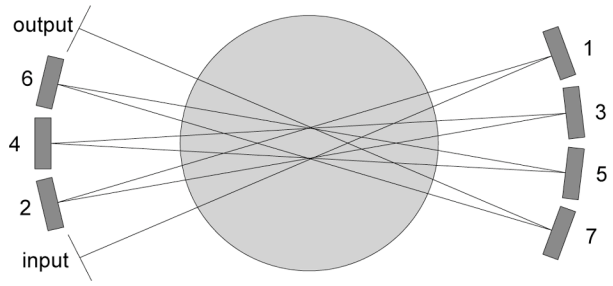

Fig. 4. Bounce pattern in the spherical Fourier cell.

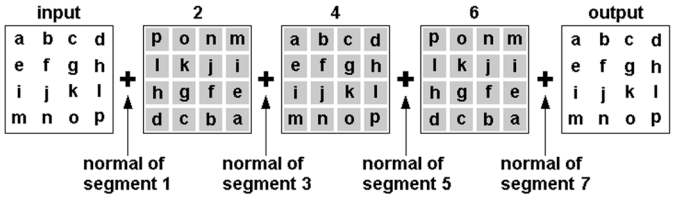

Fig. 5. Array of beams as imaged by sphere and transform mirrors.

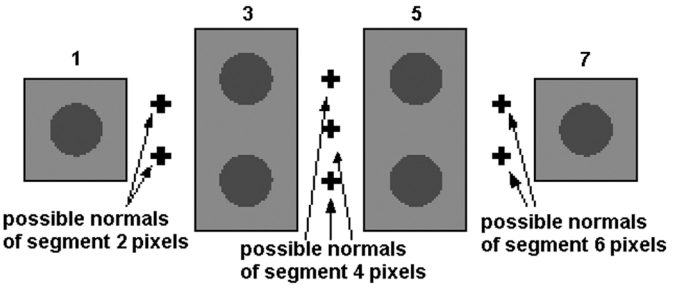

Fig. 6. Transform mirrors and incident beams.

line is the current optical axis. From the figure we can see that in terms of paraxial rays an object is imaged about the normal of a mirror in the transform plane, with the image being formed in the left focal plane of the ball lens.

If we introduce mirror segments at both the transform and object planes (all a focal distance from the center of the sphere), each with varying angles, a bounce pattern develops where the beam is incident on each segment once. In Fig. 4, a beam is present at the input with a given direction so that its transform is centered on the mirror segment 1. The normal to mirror segment 1 is between the input and segment 2, so the input is imaged onto segment 2. Segment 2 has a normal such that segment 1 is imaged onto segment 3. This pattern continues with the beam bouncing on each numbered segment in order until it reaches the output. All the even-numbered segments, as well as the output, are images of the input, and all of the odd-numbered segments are transforms of the input and are images of each other.

We have shown how a beam can work its way around a circle, alternately being Fourier-transformed and transformed back again. For true-time delay, we want the system to be able to handle an array of inputs. The input beams enter the cell from a fiber array at the input, all parallel to each other. If we consider only the center of each beam we can use rays to describe how they will propagate through the system. Fig. 5 shows the view of the input, output and even-numbered segments, as viewed from the center of the sphere. The letters indicate where the centers of sixteen different beams are located and where they are imaged on each segment (the number of beams is arbitrary; there could be any number of inputs). The plus signs show the intersection of the normals to segments on the opposite side of the spherical lens. Thus, the image of each array is reflected around the corresponding "+."

Now we can replace the flat mirrors in the image planes with MEMS devices. Each segment where the beams are imaged is replaced with a MEMS chip that is an array of micromirrors (pixels) that can tip to one of three angles, up down, or flat. The arrangement and pitch of pixels is set to match the array of inputs, such that each beam is incident on the center of one of the micromirrors on each pass. This is illustrated in Fig. 5 where segments 2, 4, and 6 are micromirror arrays (MEMS). The pixel tips will change the destination of the Fourier transform for any particular beam.

Next we look at the Fourier-transform side of the lens. In Fig. 6 we see the transform mirrors as viewed from the center of the sphere; all the odd-numbered bounces are on the Fourier transform side of the cell (shown in Fig. 6) and all of the even-numbered bounces are images of the input array (Fig. 5). All rays leaving the MEMS parallel will coincide in the Fourier planes (the odd-numbered segments). If we consider the axes of the Gaussian beams to be parallel, and each centered on a chief ray, these chief rays intersect in the Fourier plane indicating that the beams overlap there. This results in all the beams coming in from the input array overlapping at segment 1. Segment 2 (behind the viewer in Fig. 6) is a MEMS with two possible tip angles.

By tipping MEMS pixels in the object plane we can change the angle of the chief rays for some of the beams, causing them to overlap in a different position. The result is the chief rays of each beam will have one of two angles after reflecting on the MEMS array. One of the reflected angles is slightly downward causing the transform spot to be centered on the lower half of the mirror on the Fourier side. The other possible reflected angle is slightly upward, causing the transform spot to be centered on the upper half of the mirror. Any beam's transform could be located at either the top or the bottom of segment 3. Since all beams have two possible reflected angles, all the beams overlap in one of the two positions at the transform plane; these are one above the other on each Fourier mirror in Fig. 6. Both sections of segment 3 have the same normal so the beam location at 4 is not affected by whether a beam came from to the top or bottom of segment 3.

The MEMS chip at segment 4 has three possible states: flat, which images the top of 3 to the bottom of 5 or the bottom of three to the top of 5, $+\theta$ which images the top of 3 to the top of 5, and $-\theta$ which images the bottom 3 onto the bottom of 5. Possible pixel normals are shown as "+" in Fig. 6 for each segment. The dark circles indicate the locations of the beams, all of which are made to overlap for input and output at segments 1 and 7, but can be at two locations for segments 3 and 5. That is, the Fourier transforms of some or all of the beams are coincident at the top of segment 3, and the Fourier transforms of the remaining beams coming from the MEMS at segment 2 are coincident at the bottom of segment 3. At each transform location

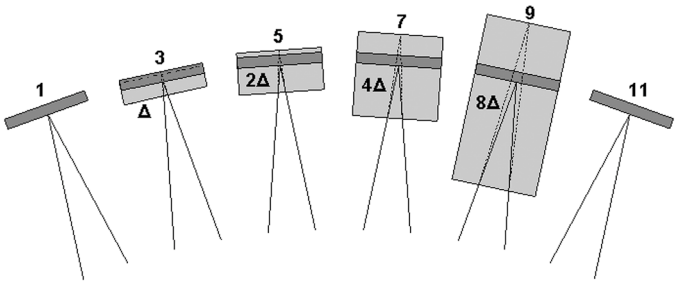

Fig. 7. Top view of transform mirrors with delay blocks added.

there are overlapping Gaussian beams that are centered about the same point. The beams are all at their waists at the MEMS pixels, but in separate locations.

B. Introducing the Time Delay Paths

In order to introduce a time delay, the bottom halves of mirror segments 3 and 5 are replaced by glass blocks or lens trains with mirrors at their ends that result in the same image location as the flat mirror, but have a longer transit time or delay than the mirror they replace. For example, a glass block creates a delay difference by increasing the physical path length in order to maintain the same imaging, and as well by slowing the speed of the light in the block.

Let the minimum delay be Δ and let that be the delay of the first Fourier plane (bottom of segment 3). To implement a binary sequence, one would make the delay at the bottom of each subsequent odd-numbered segment equal to twice that of the previous one. For example, if we would like to delay any beam an integer multiple Δ, between 0 and 15, we would have four transform segments, with delays of Δ, 2 Δ, 4Δ, and 8 Δ. Each beam can be sent to each of these 1 or 0 times, creating a total delay of 0 through 15 Δ.

Fig. 7 shows a top view of a binary system (four bits shown) implemented using glass blocks. Each block is labeled relative to the delay difference between the block and the mirror above it. At each segment there is a top plane mirror (darker) and below it a delay block (lighter). The ray paths going to the flat mirror (solid lines) and into the glass blocks (dashed lines) are also shown.

The number of delays possible N_d is related to the number of MEMS segments N_m by

$$N_d = 2^{(N_m - 1)}. \tag{3}$$

In any situation, the first and last MEMS segments are two-state (although three-state MEMS will work as well; there would just be an unused tip) and the rest would be three-state MEMS.

Fig. 8 shows the switching engine for a system having 6 bits of delay, 0 to 63Δ. The input is a two-dimensional fiber array, which is imaged onto the MEMS segments. The output could either be another fiber array, or a detector. The Fourier segments are the odd-numbered ones, with delays to be implemented. In most cases, one system does not take up the perimeter of the ball lens, so several could be cascaded around it. If we restrict the systems to one plane, so that there are no systems above or below, then we need only a slice of the central ball lens as depicted in Fig. 8(a). Fig. 8(b) shows a design in which nine

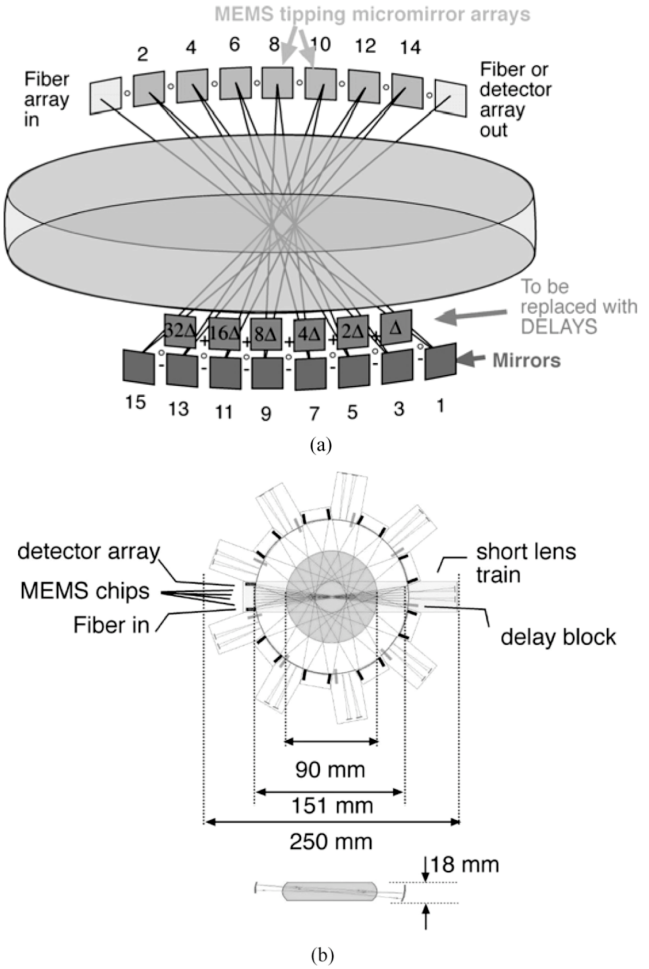

Fig. 8. (a) Switching engine for 6 bits of delay (one system). (b) Nine complete systems with 6 bits of delay each for 100 light beams sharing a single lens.

Fourier systems share a single slice of a ball lens. This design supports 900 antenna elements, with six bits of delay up to 20 ns, in a volume of 15 cubic inches.

C. Different Delay Implementations

Depending on the delay lengths and the physical size of the system there are a variety of ways in which delays can be implemented. The simplest way in which delay is added to a path is by introducing a dielectric block, similar to Fig. 7. It is necessary that the block not change the image location of the beam, while at the same time add a given amount of delay for the system. To satisfy these conditions for a given delay length the following equations apply:

$$\Delta_B = 2 \cdot l \cdot (n^2 - 1)/c \tag{4}$$

$$d_1 = l/n \tag{5}$$

where Δ_B is the additional delay associated with a block of length l and refractive index n. Here, c is the speed of light in free space and d_1 is the distance in front of the replaced mirror that the block protrudes.

The upper limit on delays possible in blocks depends upon how far in front the block can protrude before it interferes with beams visiting adjacent delay paths or null cell mirror segments.

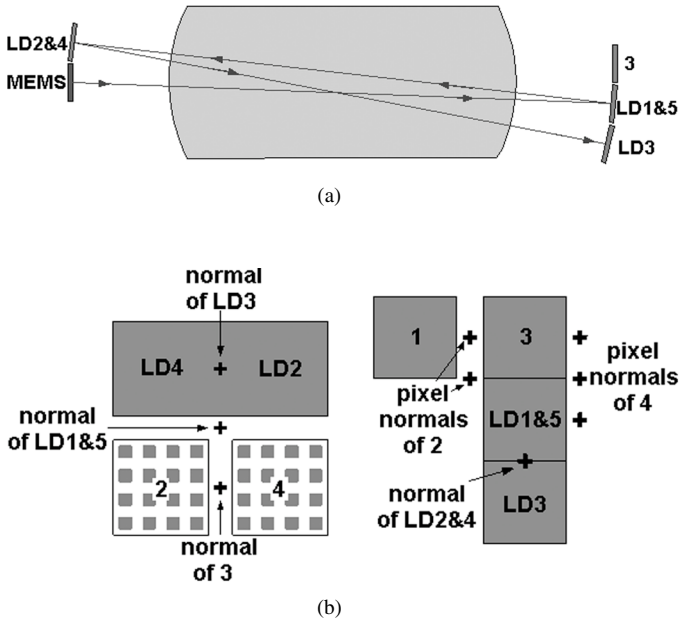

Fig. 9. (a) Segments for long delay as viewed from center of ball lens. (b) Side view of bounce progression for long delay.

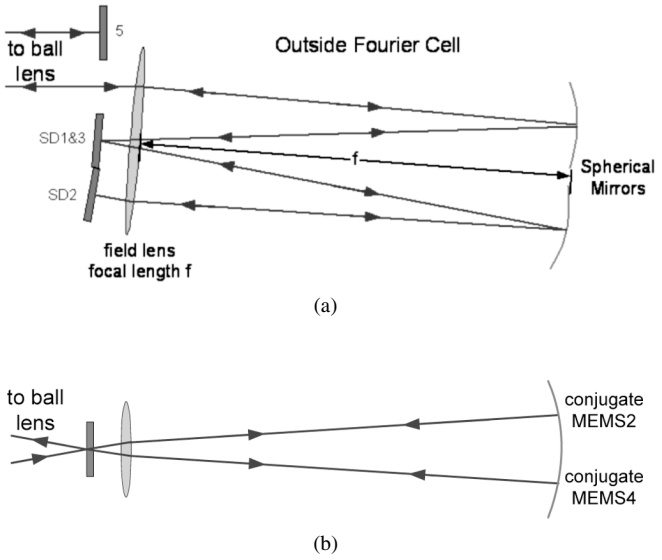

Fig. 10. (a) Side view of bounce progression for folded lens train. (b) Top view of bounce progression for folded lens train.

Dielectric blocks with higher refractive index allow for significantly longer delays.

In many cases, the delay required in a Fourier cell will be too long to be done in a dielectric block and will require longer paths with reimaging optics. To reduce space, longer delays could be folded to go through the ball lens more times.

For the longest delays that are folded back into the ball lens, it is important that they behave optically the same as the flat null cell mirror. This means that after the additional bounces that one MEMS segment is imaged with a -1 magnification onto the next MEMS segment. Fig. 9(a) shows the mirror segments of such a folded path as viewed from the center of the sphere for one of these longer delays, Fig. 9(b) shows a side view for the same delay.

If a beam did not visit the folded delay, its pixel at MEMS segment 2 would be tipped such that the beam would go to segment 3 and then be imaged with a negative magnification onto MEMS segment 4. If a beam were to receive the delay, its pixel at 2 would be tipped so that that the beam would go to segment LD1&5 on the Fourier-transform side, where there is a plain, flat mirror. Mirror LD1&5 has its normal tipped so that the negative image of MEMS 2 is incident on LD2, which is also a flat mirror. Mirror LD2 has a normal that causes LD1&5 to be imaged onto LD3. (This much of the beam path is shown in Fig. 14, it then retraces the path.) Mirror LD3 images LD2 onto LD4 (now the positive image of MEMS 2). LD2 and LD4 are part of the same mirror, meaning they have the same normal, so LD3 is imaged back onto LD1&5. Mirror segment LD1&5 has a normal that images LD4 onto MEMS 4, which is now the negative image of MEMS 2 as required. This delay has four additional round-trips through the system, which would be a minimum, but 8, 12, 16, etc. additional round-trips are also possible with the use of additional mirrors. Since the length of the delay is relative to the size of the switching engine, for a specific delay the size of the system would change.

For delays longer than the blocks, but too short to be folded back through the system, exterior folded lens trains can be used. One such lens train is shown in Fig. 10(a) and (b). Here the beam is allowed to pass by the Fourier transform segments to the outside of the system. This particular implementation requires a field lens, two spherical mirrors and two flat mirrors. For the null path the beam strikes mirror segment 5, which images MEMS segment 4 onto MEMS segment 6. If a pixel is tipped for a delay at MEMS 4 the beam passes below mirror 5 and out to the folded lens train. The beam first passes though the field lens which creates an image of MEMS 2 on the top spherical mirror [labeled as conjugate MEMS2 in Fig. 10(b)]. This spherical mirror images the entrance plane below segment 5 onto mirror SD1&3, which is tipped so that the beam now goes to the lower spherical mirror. Again, an image of the MEMS is created on the spherical mirror, this time conjugate to MEMS segment 4. This spherical mirror images SD1&3 onto SD2, but SD2 has twice the tip angle of SD1&3 so an image conjugate to MEMS 2 is created on the lower spherical mirror. Mirror SD2 is imaged back onto SD1&3, which sends the beam to the top spherical mirror creating an image conjugate to MEMS 4. Mirror SD1&3 is imaged onto the entrance plane below mirror 5 with a magnification of $+1$ (the beam exits at the same place it entered). The negative image of MEMS 2 is then incident on MEMS 4, so image location is the same whether the beam was delayed or not. In this particular example the beam travels the length of the system eight times; but any multiple of four passes is possible with the correct number and tilts of the flat mirrors.

Delays can be implemented in a variety of other optical configurations using lens trains and mirror trains with the added possibility of the entire path being inside of a dielectric. The criteria are only that delay paths do not obstruct other beam paths and image the beam similarly to the transform mirror they replace.

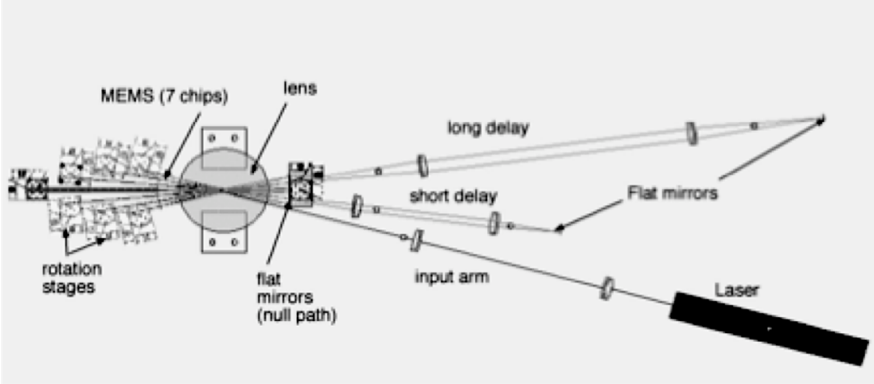

Fig. 11. Top view of experimental apparatus.

III. Experimental Apparatus

A functional Fourier cell was designed, built and demonstrated using bulk optics, Fig. 11. This design was for a six-bit system, with the longest delay arm 4 ns (maximum delay 8 ns). Only the 2 and 4 ns delays were implemented to keep costs down. In the apparatus there are seven MEMS chips on the left, each on a separate fixture for adjustment of position and tilt angle. The MEMS chips employed were residuals from another project that were creatively diced and mounted to slices of a chip carrier to allow the mirror arrays to be mounted in close proximity. Thus, on each chip only a small number of mirrors are functional. The micromirrors are 125 μm squares on a 250 μm pitch, with tip angles of $\pm 2^{\circ}$ and flat. In order to keep angles small, a ball lens radius of 50.8 mm was chosen, and that led to a focal length of 74.7 mm given the glass (BK7) had refractive index of 1.515. The disk lens in the center is the center slice of the desired ball lens, and on the right are a series of flat mirrors, the Fourier mirrors. A single input beam was used.

The Fourier mirrors were cut from a single aluminum substrate using a slow-tool-servo diamond-turning machine. This mirror array consists of all flat mirrors, Fig. 12. Here we see six flat segments, at 5 $^{\circ}$ angles with respect to adjacent segments. Two of the segments are shorter; the resulting gaps allow beams to pass to and from the two delay paths. A beam sent to the lower half of the mirrors experiences no relative delay; beams sent to the top transit through delay paths and return. The mirror angles are accurate to 0.2% (measurement-limited). The RMS surface roughness is ≈ 8.5 nm, although there were visible tool marks and a couple of scratches visible. The roughness figure just given does not include those defects.

Fig. 13 shows a close-up of the apparatus as seen from the top. The MEMS are on the left, and the Fourier mirrors are on the right. The input beam could be actively switched from the upper to lower Fourier mirrors; in the figure the beam is being sent to both delays.

Fig. 15 shows the entire apparatus. The input beam is from a HeNe laser, modulated with a 2–ns pulse. Time delays are measured on an oscilloscope. Fig. 14 shows the delays left to right for the null path, the short delay, the long delay, and a beam going to both the short and the long delays. Table I shows the expected values based on the commercial off-the-shelf lenses used, along with the measured values. All delays are accurate to within the measurement equipment limitations.

Fig. 12. Fourier mirror segments.

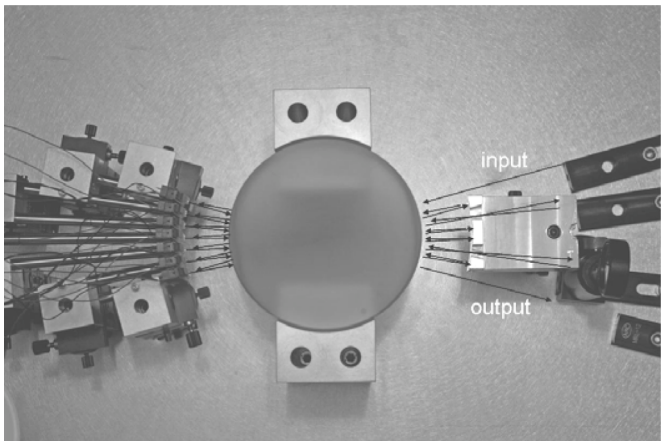

Fig. 13. Top view of system.

The loss measurements are shown in Table II. The measured losses are high primarily because of the uncoated Al mirrors both at the MEMS end and the Fourier end. The "theoretical" values represent the expected loss of the system based on surface losses and material absorption. For example, a beam following the null delay path is incident on seven MEMS pieces, which were found to be 90.5% reflective, six times on Fourier segments found to be 87.5% reflective, 28 times on the AR coated ball lens, which has coatings with transmission of 0.99, goes

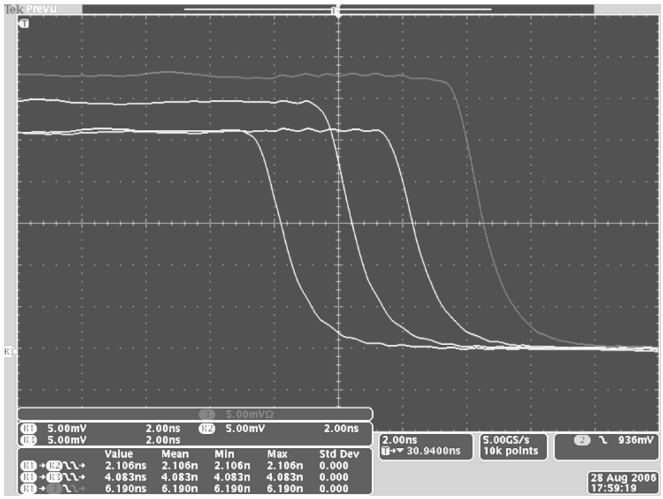

Fig. 14. Delay Measurements.

through 140 cm of BK7 with an internal transmittance per cm of 0.998, leading to a 0.127 system efficiency. The measured loss is higher than theoretical, which can be attributed to diffraction losses from aberration, defocus, and scattering off the tool marks that were evident on the Fourier mirrors. This conclusion is supported by crosstalk measurements, presented later. The modeled loss values that could be expected for a best-case implementation of our experimental system (with 1550 nm wavelength, gold-plated MEMS, improved coatings including the Fourier mirrors, lenses made of fused silica) are also given. In this case, the MEMS is taken to be 0.978 reflective, Fourier mirrors and all other surfaces are 0.999 efficient, and transmittance per cm of the glass is 0.999. The modeled best case for a full six-bit implementation, using four additional lens train delays, is 1.71 dB.

Table III gives the results of crosstalk measurements. This is a measure of the power received at a channel adjacent to an intended channel, adjacent to the left, the right, up, and down. We observe that the crosstalk is much worse in the horizontal direction. Since the tool marks on the diamond-turned Fourier mirrors were vertical, we expect diffraction in the horizontal direction, accounting for the difference. With optimization of all optical surfaces we believe that crosstalk lower than -40 dB is achievable.

Thus, we have demonstrated for the first time the operating principle of the Fourier cell, demonstrating the alignment, proper switching between delay paths, correct imaging through the disk lens, and that the proper delays can be obtained with high accuracy.

IV. Summary and Discussion

An imaging system called a spherical Fourier cell has been presented. In it, the optical Fourier transform is performed repeatedly, creating images of the input on sequentially visited MEMS arrays. The method to adapt the system to provide true time delay to an array of optical beams was described. A bulk optic demonstration was designed and built for a 6–bit system, but with only two of delay paths present. Relative delay was measured, with paths of 0, 2.1, 4.1, and 6.2 ns of delay shown. Measured loss was 12 dB or less, and the enhancements required to reduce the optical loss below 2 dB were listed. Crosstalk in the experimental setup was found to be less than -18 dB, and would clearly be less than -30 dB if scratches and tool-marks on the Fourier mirror segments were minimized. In addition, we estimate that crosstalk below -40 dB is achievable in a system with optimized optical surfaces.

In order to further reduce the size of the system more compact delay paths need to be developed. This will require a

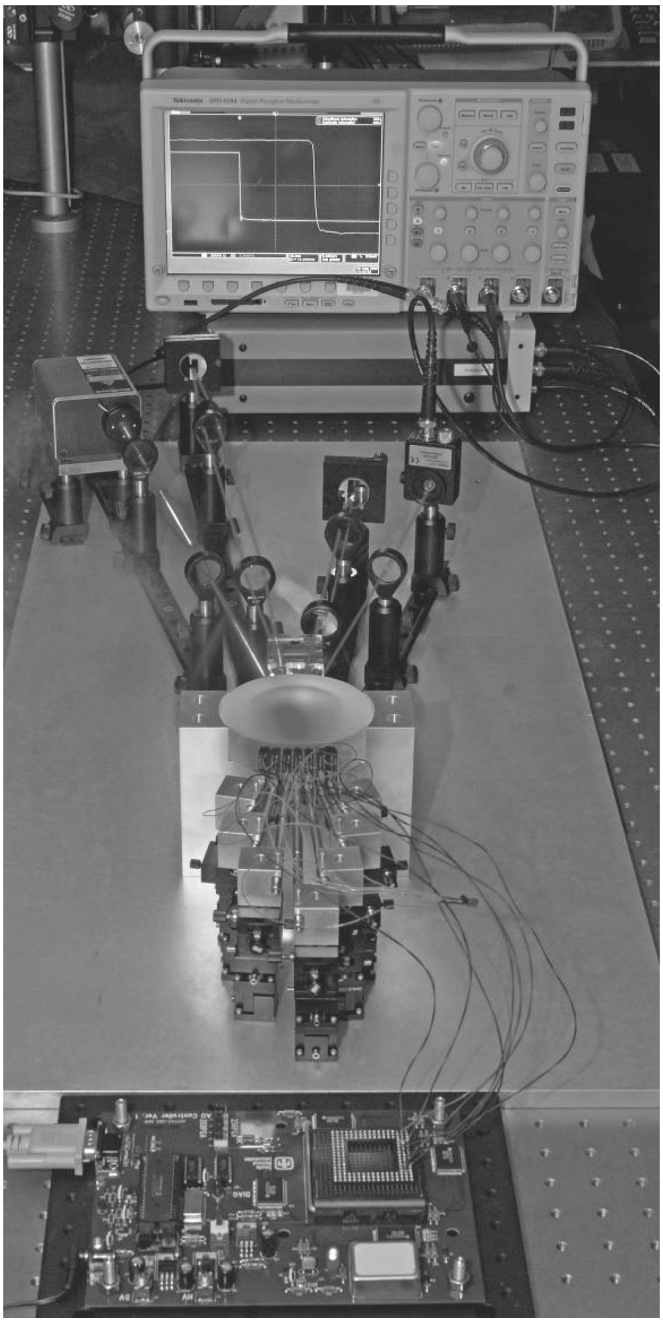

Fig. 15. System with all equipment.

TABLE I
Delay Measurements

Path	Design value (ns)	Measured (ns) (±7 ps)
Null	(ref)	(ref)
Short delay	2.11	2.106
Long delay	4.09	4.083
Both delays	6.20	6.190

TABLE II
LOSS MEASUREMENTS

	Null cell	Short Delay	Long Delay	Both Delays
Measured value	12.0 dB	11.4 dB	11.8 dB	11.0 dB
Theoretical value	8.97 dB	8.61 dB	8.61 dB	8.25 dB
Best case system	**1.45 dB**	**1.49 dB**	**1.49 dB**	**1.54 dB**

TABLE III
CROSSTALK MEASUREMENTS

	Left	Right	Up	Down
Null cell	-17.1 dB	-19.1dB	-31.3 dB	-33.8 dB
Short Delay	-17.8 dB	-19.0 dB	-33.0 dB	-33.8 dB
Long Delay	-17.9 dB	-19.8 dB	-30.1 dB	-30.4 dB
Both Delays	-20.8 dB	-20.3 dB	-32.4 dB	-34.7 dB

much more custom approach, using processes like diamond machining more extensively. Longer delay paths could possibly be folded back through the switching engine as well. Another desire is to eliminate as much of the optomechanics as possible by precision fabrication of optical surfaces which are fixed to a common surface and accurately aligned with respect to one another. Maximum achievable delays will ultimately be determined by pointing accuracy of delay optics. For example, a delay of 20 ns requires a free space path length of 6 m, or 3 m to a retro mirror and back. If the tilt accuracy of that mirror is off by 10 μrad the position at the MEMS is offset by 60 μm leading to higher loss and crosstalk.

The Fourier cell approach is intrinsically much more compact than previous approaches, because all beams (one beam for each antenna element) share the same lens and can mostly occupy the same volume. This is in contrast with fiber-based approaches, where a distinct optical path must be provided for every delay and for every element. Although wavelength-division multiplexing can help mitigate the size and component count of fiber-based systems, these require expensive tunable lasers. In our previous work with the White cell, beams also overlap in space, making White cells lighter and smaller than comparable fiber systems. The Fourier cell is more efficient still, particularly because multiple Fourier cell systems can share a single ball lens. By comparison, the Fourier cell can deliver the same capability (number of antennas supported and bits of delay) in a volume 15 times smaller than the White cell.

ACKNOWLEDGMENT

The authors would like to thank Dr. A. Yi of The Ohio State University for machining the Fourier mirrors.

REFERENCES

[1] C. D. Nordquist, W. Dyck, M. Kraus, I. C. Reines, L. Goldsmith, W. D. Cowan, T. A. Plut, F. Austin IV, P. S. Finnegan, M. H. Ballance, and C. T. Sullivan, "A DC to 10-GHz 6-b RF MEMS time delay circuit," *IEEE Microw. Wireless Compon. Lett.* , vol. 16, no. 5, pp. 305–307, May 2006.

[2] J. White, "Long optical paths of large aperture," *J. Opt. Soc. Amer.*, vol. 32, no. 2, pp. 285–288, May 1942.

[3] C. M. Warnky, R. Mital, and B. L. Anderson, "Demonstration of a quartic cell, a true-time-delay device based on the White cell," *J. Lightw. Technology.*, vol. 24, no. 10, pp. 3849–3855, Oct. 1006.

[4] B. L. Anderson, D. J. Rabb, C. M. Warnky, and F. M. Abou-Galala, "Binary optical true time delay based on the white cell: Design and demonstration," *J. Lightw. Technol.*, vol. 24, no. 4, pp. 1886–1895, Apr. 2006.

[5] S. Kunathikom, B. L. Anderson, and S. A. Collins Jr., "Design of delay elements in binary optical true-time delay devices," *Appl. Opt.*, vol. 42, no. 35, pp. 6984–6994, Dec. 2003.

[6] B. L. Anderson and R. Mital, "Polynomial-based optical true-time delay devices with microelectromechanical mirror arrays," *Appl. Opt.*, vol. 41, no. 26, pp. 5449–5461, Sep. 2002.

[7] B. L. Anderson and C. D. Liddle, "Optical true time delay for phased array antennas: Demonstration of a quadratic white cell," *Appl. Opt.*, vol. 41, no. 23, pp. 4912–4921, Aug. 2002.

[8] B. Kanack, M. Boysel, C. Goldsmith, C. Menni, G. Magel, and C. Takle, "Optical time delay network for phased arrays," in *Proc. Transit. Opt. Processors Into Syst.*, 1993, pp. 114–132.

David J. Rabb received the B.S. degree in electrical engineering from Ohio University, Athens, in 2002, and the M.S. and Ph.D. degrees in electrical and computer engineering from The Ohio State University, Columbus, in 2005 and 2008, respectively.

He is currently working for the Electro-Optic Sensors Division, Air Force Research Laboratory. His current research interests are optical signal processing, lens design for imaging and nonimaging systems, laser radar, and optical communications.

Betty Lise Anderson (M'78-SM'95) received the B.S. degree in electrical engineering from Syracuse University, Syracuse, NY, in 1978, and the M.S. and Ph.D. degrees in materials science and electrical engineering from the University of Vermont, Burlington, in 1988 and 1990, respectively.

She spent nine years in industry, including time with Tektronix, Inc., GTE Laboratories, and Draper Laboratories. She is now a professor with Department of Electrical and Computer Engineering, The Ohio State University, Columbus. Her current research interests include analog optical signal processing, devices for optical communication systems, coherence, and semiconductor devices. She is the coauthor (with R. L. Anderson) of *Fundamentals of Semiconductor Devices* (Burr Ridge, IL: McGraw-Hill, 2005).

Prof. Anderson is a member of the Optical Society of America and the American Society for Engineering Education. She is an Associate Editor for the IEEE JOURNAL OF QUANTUM ELECTRONICS. She received the Outstanding Woman in Technology Award from TechColumbus in 2006.

William D. Cowan (S'78-M'82-SM'03) received the B.S. degree in electrical engineering from the West Virginia Institute of Technology, Montgomery, in 1982. He received the M.S. degree in electrical engineering in 1984, and the Ph.D. degree in electrical engineering in 1998, both from the Air Force Institute of Technology, Wright-Patterson Air Force Base, OH.

Recently retired from the Air Force, he has more than 25 years of experience in defense-related research and development. He has been working on micromirrors and adaptive optics since 1995. He has authored more than 38 research papers in a number of diverse technical fields including; RF components, high-temperature superconductors, high-power electromagnetic effects testing, long wavelength infrared detection, adaptive optics, and MEMS. He has also written two book chapters on micromirrors for adaptive optics. He joined Sandia National Laboratories in 2003 and is a Principal Member of Technical Staff in the RF Microsystems Department.

Dr. Cowan is a member of SPIE, Tau Beta Pi, and Eta Kappa Nu.

Olga Blum Spahn received the B.S. degree from the University of Illinois, Champaign-Urbana, in 1987, and the M.S. and Ph.D. degrees from the University of California, Berkeley, in 1990 and 1992, all in electrical engineering.

In 1993, she joined Sandia National Laboratories, Albuquerque, NM. Her research interests include MEMS/photonics integration, including postprocessing, process compatibility, and fabrication. Additionally, she is involved in optical microsystem design, fabrication and testing. Her other interests include compound semiconductor-based monolithic integration of MEMS and lasers/detectors. He has more than 100 publications and conference presentations, including several invited talks and book chapters.